

# Attempts to model neutral solitons in polyacetylene by *ab initio* and density functional methods. The nature of the spin distribution in polyenyl radicals†

Thomas Bally,<sup>\*a</sup> David A. Hrovat<sup>b</sup> and Weston Thatcher Borden<sup>\*b</sup>

<sup>a</sup> Institut de Chimie Physique, Université de Fribourg, Pérolles, CH-1700 Fribourg, Switzerland

<sup>b</sup> Department of Chemistry, University of Washington, Box 351700, Seattle, WA 98195-1700, USA

Received 25th April 2000, Accepted 30th May 2000

Published on the Web 30th June 2000

Different quantum chemical methods have been examined, in order to test their abilities to model long polyenyl radicals and, in the limit, a neutral soliton in polyacetylene. For polyenyl radicals up to C<sub>9</sub>H<sub>11</sub>, it was possible to use a range of methods up to CCSD(T). A number of interesting features of the geometries and spin distributions were found in these radicals. Coupled cluster methods reproduced rather well the experimental ratios of the spins at each of the carbons in allyl, pentadienyl, and heptatrienyl radicals. In contrast, both restricted and unrestricted Hartree–Fock methods gave very poor results. CASSCF gave good geometries and  $\pi$  spin distributions, but only if all the  $\pi$  MOs were included in the active space. Both pure (BLYP) and hybrid (B3LYP) DFT methods were found to over-estimate the widths of solitons in long polyenyl chains.

## 1. Introduction

Ever since the first successful synthesis of free-standing, high quality, polyacetylene films<sup>1</sup> and the subsequent demonstration of metallic conductivity upon their oxidative or reductive doping,<sup>2</sup> there has been an explosive interest in conjugated polymers, both in basic and in applied research. Although other electrically conductive polymers, such as polyaniline and polythiophene,<sup>3</sup> have proven to be more useful for practical applications, polyacetylene (PA) continues to stand at the focus of extensive experimental and theoretical research.<sup>4</sup>

An interesting property of pristine PA is that it shows a strong EPR signal, indicating the formation of neutral radicals during its synthesis.<sup>5</sup> Possibly due to crosslinking of the PA chains with uneven numbers of carbon atoms are apparently formed. During the initial phases of doping, this EPR signal disappears;<sup>6</sup> *i.e.*, the polyenyl radicals are either oxidized or reduced to polyenyl cations or anions, respectively. In the presence of an electric field, the resulting charges show a degree of mobility which expresses itself as conductivity in macroscopic samples of PA.<sup>7</sup>

Unlike chemists, solid-state physicists like to view the above spin or charge-carrying segments of PA as perturbations or, as they call them, “excitations” in very long or infinite (CH)<sub>n</sub> PA chains. Such an excitation can be described as a solitary wave of fixed shape which can move along PA chains. Such spin- or charge-density waves are classified as “quasi-” or “pseudo-particles” and termed solitons.<sup>8</sup> EPR experiments allow “pinned” solitons to be distinguished from mobile solitons. Although instantaneously localized to finite regions of long, conjugated PA chains, mobile solitons, as their name implies, can move along the chain in time.

One of the questions which has occupied a central place in recent experimental and theoretical research on solitons in PA and in other conjugated polyenes concerns the shape of these waves. The widths of solitons, in terms of the numbers of

carbon atoms over which they spread, has been probed by different forms of electron–nuclear double and triple resonance spectroscopy. These experiments yielded a half-width‡ of about 18 carbon atoms for a neutral soliton in all-*trans*-PA.<sup>9</sup> Another important quantity that defines the shapes of solitons and which can be probed by such experiments is the ratio of the peak values of the positive and negative spin densities. This ratio was found to be about 0.44 in all-*trans*-PA.<sup>9</sup>

Interest in using theory to model polyenes and polyenyl radicals dates back to the early days of quantum chemistry.<sup>10</sup> It was found early on that scaling of the parameter  $\beta$  with bond lengths is required in Hückel theory, in order to model correctly the electronic structure of polyenes<sup>11</sup> as well as polyenyl radicals and ions. In a seminal paper, Pople and Walmsley introduced the notion of polyenyl radicals as “defects” arising by thermal excitations in an infinitely large cyclic polyene.<sup>12</sup> This idea was later taken up by Su, Schrieffer and Heeger (SSH).<sup>8</sup> They proposed a model, which is functionally equivalent to the variable- $\beta$  Hückel method,<sup>11,13</sup> in order to describe solitons and the dynamics of their motions along infinite polyene chains.

The SSH model permitted the modelling of a number of important features of solitons in PA, such as their mobility, which depends mainly on the effects of electron–phonon interactions. However, the limitations of this model became apparent through various experiments. Among these experiments were the above-mentioned electron paramagnetic resonance measurements, which demonstrated the occurrence of both positive and negative spins on the hydrogen atoms in PA.<sup>9</sup> This finding cannot be described by Hückel-type models, because they ignore Coulombic repulsion between electrons and, hence, the electron correlation engendered by it. Both the repulsion and the correlation it engenders are treated collectively as “electron correlation” by solid-state physicists. Electron correlation is responsible for the spin polarization that

† Electronic Supplementary Information available. See <http://www.rsc.org/suppdata/cp/b0/b003288n/>

‡ By “half-width” we mean the width at half height, *i.e.* the number of carbon atoms around the center of the soliton at which the spin density is at least 50% of the maximum value.

gives rise to negative spin densities.<sup>14</sup> Within the SSH model, spin polarization is accounted for by the addition of a parameter  $U$  that represents the effects on the “on-site, electron–electron interaction”.

There has been much discussion in the solid-state physics literature as to whether electron repulsion and correlation in PA can and should be treated by perturbation theory or whether they must be included explicitly in a variational calculation.<sup>8,15</sup> However, all the calculations described in this paper contain electron repulsion explicitly; so we shall not be concerned with this question.

In this paper we focus on how well modern *ab initio* quantum chemical models, which contain no empirical parameters, are likely to perform in reproducing the properties of the neutral soliton in PA. The performance of these methods in this context depends on how well they treat electron correlation in very long polyenyl radicals. Unfortunately, the most sophisticated of these computational methods cannot currently be applied to radicals larger than nonatetraenyl. However, the results obtained by these methods for  $C_9H_{11}$  and smaller polyenyl radicals serve as benchmarks against which the performance of other computational methods that are applicable to larger polyenyl radicals can be judged.

Calculations based on density functional theory (DFT) frequently give results that are as good or better than many *ab initio* methods, and DFT calculations require only a small fraction of the computational resources of the most sophisticated *ab initio* methods. It might be hoped that DFT would provide a means of performing highly accurate calculations on polyenyl radicals whose size approaches or exceeds that of a soliton in PA. The results reported in this paper provide information as to how well DFT methods, based on two currently popular functionals, do in comparison to various *ab initio* methods in calculations on small and medium-sized polyenyl radicals and how successful the two DFT methods are in computing the properties of a soliton in PA.

## 2. Previous studies

Before discussing our results, we should point out that this study does not represent the first attempt to model the soliton in PA by *molecular* (as opposed to *solid-state*) quantum chemical methods that include the effects of electron repulsion and electron correlation. In 1983, Boudreaux *et al.* reported the results of semiempirical MNDO calculations of bond-length alternation in neutral and charged polyenes and polyenyls.<sup>16</sup> For the neutral radicals the “half-electron” scheme of Dewar *et al.*<sup>17</sup> was employed. These calculations led to a predicted half-width of the neutral soliton in PA of about 9 carbon atoms, only about 50% of the value of 18 carbons obtained from the experiments described by Kuroda.<sup>9</sup>

In a recent series of studies of reorganization energies on oxidation or reduction of polyenes and polyenyls, Rodriguez-Monge and Larsson also carried out calculations on polyenyl radicals, up to  $C_{11}H_{13}$  by UHF/UHF2, and for  $C_{23}H_{25}$  by UHF/PM3.<sup>18</sup> These methods predicted the width of the soliton invariably equal to the length of the polyenyl chain, minus 2–3 terminal carbon atoms. This failure of UHF based models had already been noted earlier by Villar and Dupuis, who showed that a qualitatively correct description of polyenyl radicals up to  $C_{11}H_{13}$  may be obtained from complete active space (CASSCF) calculations.<sup>19</sup>

In 1991, Sim *et al.* presented the first calculations on the same polyenyl radicals by a density functional method.<sup>20</sup> Within the local spin density (LSD) approximation, they obtained results which they described as being “in close accord with the CASSCF results.” However, a closer inspection shows that the C–C bond-length alternation is much less pronounced in LSD-DFT than in CASSCF, a point to which we will return in describing the results of our own study.

## 3. Quantum chemical methods

The geometries of the  $C_3$ – $C_9$  polyenyl radicals were optimized within  $C_{2v}$  symmetry by the UHF, ROHF, CASSCF, UBLYP, UB3LYP and UQCISD methods, using the GAUSSIAN 98 suite of programs,<sup>21</sup> by full- $\pi$  CASSCF with the MOLCAS programs,<sup>22</sup> and by the RCCSD, RCCSD(T) and UCCSD(T) coupled-cluster methods, as implemented in the ACES II programs.<sup>23</sup> Longer polyenyl radicals were only optimized by UHF, ROHF, UBLYP and UB3LYP, except for  $C_{11}$  and  $C_{13}$ , which were also optimized by full- $\pi$  CASSCF calculations. For the sake of consistency, the 6-31G\* basis set was used throughout. Mulliken spin populations were evaluated from the wavefunctions obtained with the different methods. Contributions from inner and outer basis functions of a given type (*i.e.*  $2p_x$ ) were added to obtain the total spin population in each atomic orbital (AO).

## 4. Results and discussion

Modelling of the soliton in PA, with its experimental half-width of about 18 carbon atoms, requires calculations on polyenyl radicals that are at least twice as long. However, we began our study with an assessment of the performance of different current quantum chemical methods in calculations on polyenyl radicals with up to 9 carbon atoms. For radicals of this size some comparisons with experimental findings can be made. In addition, “state-of-the-art” calculations by coupled-cluster methods can be performed to provide benchmarks, against which the results from other computational methods can be judged. We begin the discussion of our results with the allyl radical, the smallest polyenyl radical.

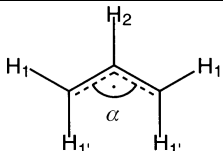
### 4.1. Assessment of the different methods in calculations on the allyl radical

The allyl radical has been the subject of numerous experimental and theoretical studies.<sup>14,24</sup> All methods employed in our study reproduce rather well the experimental geometry of the allyl radical.<sup>25</sup> However, some small differences between the results obtained by the different methods are notable (*cf.* Table 1). For example, ROHF, the only method which does not include correlation between electrons of opposite spin, predicts the C–C bond length of allyl to be slightly shorter than any other method does and shorter than is found experimentally. The same bond length is predicted to be too long by DFT with the UBLYP functional. The best overall agreement with the experimental geometry is obtained with the UB3LYP functional. As we have noted elsewhere,<sup>14</sup> this method is rather reliable for geometry optimizations of open-shell species.

The differences between different computational methods become much more evident when one compares the predicted *spin distributions* in the allyl radical (see Table 2). However, in considering how best to compare the spin distributions, computed by different methods, with each other and with experiments, a question arises; and the answer to this question will be important for the rest of our study. Which calculated spin densities should be compared, those in the  $2p_x$  AOs of the carbons or those at the hydrogen nuclei?

For comparing the width calculated for a soliton with the experimental value, it might seem that the atomic spin populations in the  $2p_x$  AOs on the carbons would be most appropriate. However, in experimental determinations of spin distributions it is the hyperfine coupling constants to the hydrogens ( $a_H$ ) that are usually measured. The  $a_H$  values are proportional to the spin *densities* at the hydrogen nuclei, which are dominated by the spin *populations* in the 1s AOs.

However, according to a relationship proposed by McConnell,<sup>26</sup> the  $a_H$  values in open-shell, planar,  $\pi$  systems are proportional to the spin populations in the  $2p_x$  AOs of the carbon

**Table 1** Bond lengths (in Å) and C–C–C bond angle (in °) of the allyl radical according to different methods (all with the 6-31G\* basis set)


	Exp. <sup>a</sup>	ROHF <sup>b</sup>	UHF	CASSCF <sup>c</sup>	UBLYP	UB3LYP	RCCSD	RCCSD(T)	UQCISD	UCCSD(T)
$r_{\text{C-C}}$	1.387	1.372	1.391	1.390	1.395	1.386	1.389	1.393	1.390	1.392
$r_{\text{C-H}_1}$	1.091	1.078	1.078	1.078	1.098	1.091	1.091	1.093	1.091	1.093
$r_{\text{C-H}_2}^d$	1.084	1.074	1.075	1.074	1.093	1.086	1.086	1.089	1.087	1.089
$\alpha^e$	124.7	124.5	124.5	124.7	125.3	125.1	124.3	124.3	124.3	124.3

<sup>a</sup> From Hirota *et al.*<sup>25</sup> <sup>b</sup> Note that the allyl radical is unstable with regard to geometric distortion at the ROHF level. <sup>c</sup> With a full  $\pi$  (3,3) active space. <sup>d</sup> Averaged over the two terminal C–H bond lengths;  $\text{C}_1\text{--H}_1$  is computed to be shorter than  $\text{C}_1\text{--H}_1'$ , by 0.002 Å by all our calculations. <sup>e</sup> The H–C–H and H–C–C angles are predicted within 0.2° of each other by all methods.

atom to which each of the hydrogen atoms is bonded. This useful relationship made it possible to analyze the EPR spectra of numerous planar  $\pi$  radicals and radical ions by means of simple Hückel-type calculations on the systems.<sup>27</sup> If the McConnell relationship were strictly obeyed by the *calculated*  $2p_\pi(\text{C})$  spin densities and the *calculated* hydrogen coupling constants, it would not matter which of these two sets of quantities from different calculations were compared, because the carbon  $2p_\pi(\text{C})$  spin densities would be proportional to the  $a_{\text{H}}$  values.

Computed  $1s(\text{H})$  and  $2p_\pi(\text{C})$  spin populations, obtained from Mulliken-type analyses of the wavefunctions from our calculations on the allyl radical are given in Table 2. Also listed are the total atomic spin populations on each of the carbon atoms and the calculated  $a_{\text{H}}$  values. The ratios of the spin populations in the  $2p_\pi$  AOs on the terminal and central carbons and in the  $1s$  AOs of the hydrogens attached to these carbons in the allyl radical are also provided in Table 2, along with the ratios of the hyperfine coupling constants for the hydrogens. This table reveals a number of features that are largely independent of computational method. For example, as expected, the computed ratios of the hyperfine coupling constants for the hydrogens attached to  $\text{C}_1$  and  $\text{C}_2$  are quite close to the ratios of the spin densities in the  $1s$  AOs of these hydrogens. The ratios of the  $a_{\text{H}}$  values are 3–7% smaller than the ratios of the  $1s(\text{H})$  spin populations, presumably because the spins in the  $\sigma$ -AOs on the carbon atoms contribute slightly to the calculated spin densities at the hydrogen nuclei.

Table 2 shows that the *total* spin population at each carbon atom is significantly larger in magnitude than the spin population in the  $2p_\pi$  AO of that carbon. The reason is that the unpaired electron spin in the  $2p_\pi$  AO polarizes the spins of the electrons in the  $\sigma$  bonds to that carbon, so that electrons of

the *same* spin tend to appear in the  $\sigma$  and in the  $2p_\pi$  AOs of each carbon.<sup>28</sup> Because the Pauli principle prevents electrons of the same spin from simultaneously appearing in the same region of space, spin polarization of the electrons in the  $\sigma$  AOs by the unpaired spins in the  $2p_\pi$  AOs minimizes the Coulombic repulsion energy between the  $\sigma$  and  $\pi$  electrons.

The polarization of the electrons in the C–H bonds by the unpaired spins in the  $2p_\pi$  AOs results in spin density appearing in hydrogen  $1s$  AOs, despite the fact that these AOs lie in the nodal plane of the  $2p_\pi$  AOs. Because the spin in each  $1s$  AO is opposite in sign to the spin that appears in the  $2p_\pi$  AO of the carbon to which the hydrogen is attached, spin polarization is responsible not only for the non-zero values of  $a_{\text{H}}$  but also for the fact that the sign of  $a_{\text{H}}$  is different for hydrogens attached at different carbons. For protons attached to a carbon that has a positive spin density in its  $2p_\pi$  AO,  $a_{\text{H}}$  has a negative sign, and for protons attached to a carbon that has a negative spin density in its  $2p_\pi$  AO,  $a_{\text{H}}$  has a positive sign.

Spin polarization is also responsible for the appearance of spin in the  $2p_\pi$  AO of the central carbon ( $\text{C}_2$ ) of the allyl radical, where the singly occupied, non-bonding (NB)MO has a node. The spin in the  $2p_\pi$  AO of  $\text{C}_2$  is opposite in sign to that in the  $2p_\pi$  AOs of  $\text{C}_1$  and  $\text{C}_3$ ; since, if there is an  $\alpha$  spin electron in the NBMO, the  $\beta$  spin electron in the bonding MO can avoid appearing in the same region of space as the electron in the NBMO by becoming more localized at  $\text{C}_2$ , where the NBMO has a node.<sup>14</sup>

An important test of the computational results in Table 2 is how well each method predicts the ratio of the negative spin density in the  $2p_\pi$  AO of  $\text{C}_2$  to the positive spin density in the  $2p_\pi$  AO of  $\text{C}_1$ . If the McConnell relationship holds, this calculated ratio should be the same as the calculated ratio of computed hydrogen hyperfine coupling constants. However, if

**Table 2** Spin populations and  $^1\text{H}$  hfc constants for allyl radical by different methods

	Atomic spin populations			Spin in $2p_\pi$			Spin in H $1s$ AOs			$^1\text{H}$ hfc constants $a_{\text{H}}^a$		
	$\text{C}_2$	$\text{C}_1$	$\text{C}_2/\text{C}_1$	$\text{C}_2$	$\text{C}_1$	$\text{C}_2/\text{C}_1$	$\text{H}_2$	$\text{H}_{1/1'}$ <sup>b</sup>	$\text{H}_2/\text{H}_{1/1'}$	$\text{H}_2$	$\text{H}_{1/1'}$ <sup>b</sup>	$\text{H}_2/\text{H}_{1/1'}$
ROHF <sup>c</sup>	0.000	0.500	0.000	0.000	0.500	0.000	—	—	—	—	—	—
UHF	−0.793	1.025	−0.773	−0.522	0.758	−0.688	0.049	−0.077	−0.642	24.13	−36.43	−0.662
CASSCF <sup>d</sup>	−0.198	0.599	−0.330	−0.206	0.600	−0.343	—	—	—	—	—	—
UBLYP	−0.197	0.655	−0.301	−0.132	0.562	−0.234	0.008	−0.030	−0.256	3.59	−14.62	−0.246
UB3LYP	−0.279	0.703	−0.398	−0.194	0.594	−0.328	0.011	−0.033	−0.339	5.37	−16.43	−0.327
RCCSD	−0.334	0.750	−0.445	−0.209	0.594	−0.352	0.015	−0.045	−0.337	6.76	−20.60	−0.328
RCCSD(T)	−0.290	0.726	−0.400	−0.178	0.577	−0.308	0.012	−0.043	−0.282	5.36	−19.67	−0.272
UQCISD	−0.343	0.754	−0.455	−0.222	0.600	−0.369	0.012	−0.044	−0.281	5.22	−19.95	−0.261
UCCSD(T)	−0.287	0.723	−0.397	−0.180	0.578	−0.311	0.010	−0.042	−0.236	4.18	−19.05	−0.219
Experiment	—	—	—	—	—	—	—	—	—	4.06	−14.38	−0.282

<sup>a</sup> In Gauss. <sup>b</sup> Averaged over the two terminal H atoms (they differ by about 1 G). <sup>c</sup> Due to the absence of spin polarization in this model, there is no spin on the central C or on the H atoms. <sup>d</sup> With a full  $\pi$  (3,3) active space. As no  $\sigma$ -MOs are in the active space, no spin appears on the H atoms.

these two ratios differ, then one has to decide which of them to compare with the experimental ratio of hyperfine coupling constants.

The experimental  $a_H$  values for the allyl radical are given in Table 2, along with those computed by the different computational methods that we examined. The DFT methods (UBLYP and UB3LYP) both give good absolute values of the hyperfine coupling constants, as has been noted previously for allyl and other radicals.<sup>29</sup> However, the average  $a_H$  value for the two different hydrogens at  $C_1$  is substantially overestimated by all the coupled-cluster calculations, as well as by the closely related UQCISD method. This failure of these highly sophisticated methods is surprising, since one would have expected that they should be capable of computing the hyperfine coupling constants in the allyl radical correctly.

The reason for this failure is that these methods apparently overestimate the amount of polarization of the electrons in the C–H bonds by the spins in the  $2p_\pi$  AOs. If the spin density at each hydrogen were overestimated by a constant factor, the constant could be eliminated by computing the *ratio* of the  $a_H$  values for the hydrogens attached to  $C_1$  and  $C_2$  (see the last column of Table 2).

Despite the fact that the UBLYP and UB3LYP values for the individual hyperfine coupling constants are in much better agreement with experiment than the RCCSD(T) and UQCISD values, the RCCSD(T) and UQCISD ratios of coupling constants are closer than the UBLYP and UB3LYP ratios to the experimental one of  $-0.282$ . However, the UCCSD(T) ratio of hyperfine coupling constants is 30% smaller in magnitude than the experimental value.

It is interesting to note that, although UB3LYP, RCCSD(T) and UCCSD(T) give very different ratios of hydrogen hyperfine coupling constants, these methods all give spin densities in the carbon  $2p_\pi$  AOs that are not only very close to each other but also to the CASSCF values. In addition, the ratios of these  $2p_\pi$  spin densities are all reasonably close to, although 10–15% higher than the ratios of the experimental  $a_H$  values. We interpret these findings as indicating that all four of these methods do give reasonably accurate  $2p_\pi$  spin densities, but that they differ in how well the amount of  $\pi$ – $\sigma$  spin polarization is computed by them.

The UHF-based coupled cluster methods [UCCSD(T) and UQCISD] seem to perform particularly badly in this regard. Both methods give a calculated ratio of  $a_H$  values that is 30% smaller in magnitude than the calculated ratio of  $2p_\pi$  spin densities. The difference between these two ratios represents a large deviation from the McConnell relationship, which predicts that the ratio of hydrogen hyperfine coupling constants should be the same as the ratio of  $2p_\pi$  spin densities.

In contrast, the UBLYP and UB3LYP ratios of the  $2p_\pi$  spin densities and of the  $a_H$  values are virtually identical, as expected from the McConnell relationship. The ratios of  $2p_\pi$  spin densities and of the  $a_H$  values differ, when computed at RCCSD and RCCSD(T) levels, but only by 7–10%. The good agreement between these ratios shows that at these levels of theory the McConnell relationship is at least semi-quantitatively correct. This finding provides computational justification for using the McConnell relationship to deduce  $2p_\pi$  spin densities from hyperfine coupling constants that are measured experimentally, and *vice versa*.

The results in Table 2 for the allyl radical indicate that methods, such as UCCSD(T), which appear to give rather accurate ratios of  $2p_\pi$  spin densities, do not necessarily give good ratios of  $a_H$  values. Therefore, in assessing how well different computational methods describe the width of a soliton in PA and the degree to which the unpaired electron is delocalized in smaller polyenyl radicals, it seems wiser to focus on the ratios of the calculated  $2p_\pi$  spin densities, rather than on the ratios of the calculated hyperfine coupling constants. In radicals for which ratios of experimental hyperfine coupling

constants are available, the McConnell relationship justifies using these ratios to deduce the experimental ratios of  $2p_\pi$  spin densities, with which the calculated ratios can be compared. Comparisons of this type are made in the next section for three radicals—pentadienyl, heptatrienyl and nonatetraenyl—that are higher vinyls of allyl.

## 4.2. Results of calculations on pentadienyl, heptatrienyl and nonatetraenyl radicals

Table 3 lists the geometries of the  $C_5$ – $C_9$  polyenyl radicals, obtained by different methods; and Fig. 1 shows a graphical representation of the degree of bond-length alternation (*i.e.*, the difference between the lengths of adjacent C–C bonds) for these species. Since no experimental geometries are available for these radicals, we can only compare the geometries obtained by different methods among each other.

We will not comment on the *absolute* values of the C–C bond lengths listed in Table 3 (which differ by less than 0.02 Å between the methods, if we disregard the single-determinant SCF models), but focus instead on the *differences* between adjacent bond lengths, *i.e.*, the degree of bond-length alternation.

These are represented graphically in Fig. 1 from which it becomes immediately evident that the ROHF method (column a for all three radicals) predicts up to twice as much bond-length alternation as any of the other methods. The absence of electron correlation from the wave function prevents the unpaired electron from delocalizing along the polyenyl chain, since keeping this electron confined to the central carbons of each radical minimizes its interactions with the other  $\pi$  electrons.<sup>5</sup> Consequently, bond-length alternation near the terminal carbons rapidly approaches that found in polyenes (about 0.15 Å). The opposite happens at the UHF level (column b for each radical), where the bond-length alternation is always much smaller than that found by the other methods.

The differences between the amounts of bond-length alternation predicted by the CASSCF, DFT and coupled cluster

**Table 3** Geometries of  $C_5$ – $C_9$  polyenyl radicals by different methods<sup>a</sup>

Molecule	Method	$r_1^b$	$r_2^b$	$r_3^b$	$r_4^b$
$C_5H_7$	ROHF	1.333	1.435		
	UHF	1.374	1.415		
	CASSCF	1.367	1.421		
	UBLYP	1.376	1.422		
	UB3LYP	1.366	1.415		
	UQCISD	1.367	1.421		
	RCCSD	1.364	1.422		
	RCCSD(T)	1.371	1.421		
	UCCSD(T)	1.369	1.422		
$C_7H_9$	ROHF	1.329	1.447	1.377	
	UHF	1.370	1.421	1.400	
	CASSCF	1.358	1.436	1.394	
	UBLYP	1.369	1.432	1.401	
	UB3LYP	1.358	1.426	1.392	
	UQCISD	1.356	1.437	1.393	
	RCCSD	1.355	1.437	1.393	
	RCCSD(T)	1.363	1.436	1.397	
	UCCSD(T)	1.359	1.437	1.395	
$C_9H_{11}$	ROHF	1.326	1.457	1.344	1.423
	UHF	1.369	1.423	1.396	1.407
	CASSCF	1.353	1.445	1.379	1.412
	UBLYP	1.366	1.437	1.393	1.412
	UB3LYP	1.354	1.432	1.381	1.405
	UQCISD	1.351	1.446	1.378	1.411
	RCCSD	1.351	1.446	1.376	1.412
	RCCSD(T)	1.358	1.443	1.384	1.412

<sup>a</sup> Geometries optimized with the 6-31G\* basis set within  $C_{2v}$  symmetry by the method indicated in the second column. <sup>b</sup> In Å, see Fig. 1 for designation of bonds.

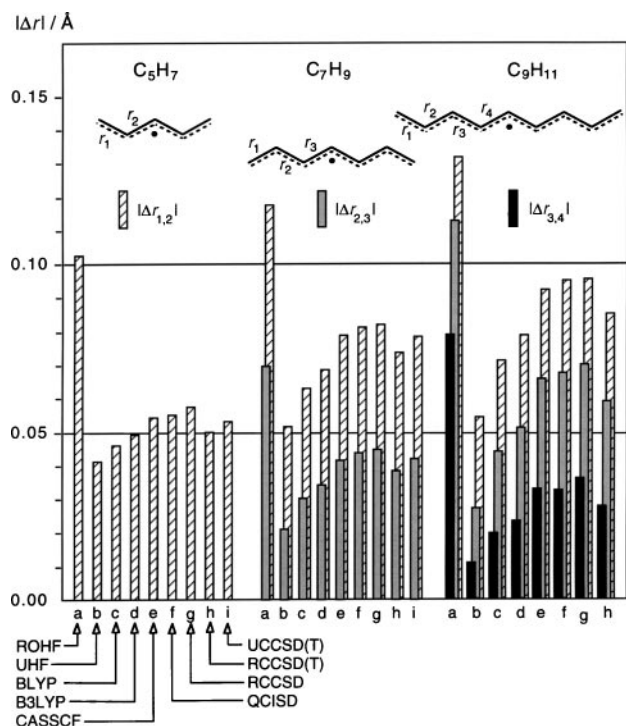


**Fig. 1** Bond-length alternation in  $C_5H_7$ ,  $C_7H_9$  and  $C_9H_{11}$  by different methods. Hashed bars denote difference between  $r_1$  and  $r_2$  (see drawing above plot), gray bars the difference between  $r_2$  and  $r_3$  (for  $C_7H_9$  and  $C_9H_{11}$ ), and black bars that between  $r_3$  and  $r_4$  (for  $C_9H_{11}$  only).

methods are more subtle. The CASSCF predictions (column e) are close to those made by the QCISD and coupled-cluster calculations (columns f–i); whereas, the DFT methods predict less bond-length alternation. The amount of alternation predicted by UBLYP for each radical (column d) is slightly less than that predicted by the hybrid UB3LYP functional

(column e), and UB3LYP predicts a degree of bond-length alternation that is only slightly smaller than that predicted by RCCSD(T). The gradient-corrected exchange functionals in UBLYP and UB3LYP appear to give better results than the exchange functionals that use the local spin density (LSD) approximation, which were employed in previous DFT calculations on polyenyl radicals.<sup>20</sup>

As in the case of the allyl radical, the differences between the methods tested for the  $C_5$ – $C_9$  polyenyl radicals become more evident when one looks at the calculated spin distributions, rather than the bond lengths. As discussed in the previous section, the best comparisons to make are of the relative spin populations in the  $2p_\pi$  AOs of the carbon atoms. These are listed for  $C_5$ – $C_9$  in Table 4, where the spin population is arbitrarily set to one for the carbon atom that bears the most spin.

If one assumes that the McConnell relationship holds for  $C_5H_7$ <sup>30</sup> and  $C_7H_9$ ,<sup>31</sup> the ratios of the  $2p_\pi$  spin populations at different pairs of carbons can be deduced from the ratios of the experimental hydrogen hyperfine coupling constants,  $a_H$ . The “experimental” ratios of  $2p_\pi$  spin densities obtained in this way can then be compared with the calculated ratios.

UBLYP and UB3LYP both appear to predict too much spin at the terminal carbon atoms, which suggests that these methods have a tendency to overestimate the delocalization of the unpaired electron in polyenyl radicals. However, the deviations of these DFT methods from experiment are not nearly as bad as that of the UHF model, which greatly overestimates the amounts of positive and negative spin densities and predicts more unpaired spin at the terminal than at the interior carbons!

As we have pointed out,<sup>14</sup> this overestimation of spin polarization is a direct consequence of the admixture of high-spin states into the UHF wavefunctions. The presence of these states reveals itself in the strong deviation of the expectation value of the  $S^2$  operator for the UHF wavefunctions from the theoretical value of  $\langle S^2 \rangle = 0.75$  for pure doublets. Indeed, the value of  $\langle S^2 \rangle = 1.838$  for the UHF wavefunction for  $C_9H_{11}$  is closer to that for a triplet ( $\langle S^2 \rangle = 2.0$ ) than for a doublet. The

**Table 4** Relative  $2p_\pi$  spin populations of  $C_5$ – $C_9$  polyenyl radicals by different methods<sup>a</sup>

Molecule	Method	$C_1$	$C_2$	$C_3$	$C_4$	$C_5$	$\langle S^2 \rangle^b$
$C_5H_7$	UHF	1.05	−0.80	1.00			1.219
	CASSCF <sup>c</sup>	0.75	−0.31	1.00			0.750
	UBLYP	1.00	−0.26	1.00			0.770
	UB3LYP	0.96	−0.37	1.00			0.799
	UQCISD	0.81	−0.38	1.00			—
	RCCSD	0.77	−0.34	1.00			0.760
	RCCSD(T)	0.83	−0.32	1.00			0.747
	UCCSD(T)	0.80	−0.31	1.00			0.747
	Experiment <sup>e</sup>	0.86	−0.28	1.00			0.750
	$C_7H_9$	UHF	1.06	−0.82	1.00	−0.90	
CASSCF <sup>c</sup>		0.64	−0.30	1.00	−0.42		0.750
UBLYP		0.96	−0.26	1.00	−0.31		0.772
UB3LYP		0.91	−0.37	1.00	−0.46		0.814
UQCISD		0.73	−0.38	1.00	−0.53		— <sup>d</sup>
RCCSD		0.67	−0.33	1.00	−0.47		0.767
RCCSD(T)		0.72	−0.30	1.00	−0.42		0.746
UCCSD(T)		0.70	−0.30	1.00	−0.43		0.750
Experiment <sup>e</sup>		0.79	−0.28	1.00	−0.35		—
$C_9H_{11}$		UHF	1.08	−0.84	1.02	−0.94	1.00
	CASSCF <sup>c</sup>	0.47	−0.24	0.81	−0.39	1.00	0.750
	UBLYP	0.91	−0.26	0.96	−0.32	1.00	0.774
	UB3LYP	0.84	−0.36	0.94	−0.48	1.00	0.830
	UQCISD	0.62	−0.34	0.89	−0.55	1.00	— <sup>d</sup>
	RCCSD	0.62	−0.32	0.80	−0.44	1.00	0.775
	RCCSD(T)	0.66	−0.30	0.88	−0.42	1.00	0.746
	UCCSD(T) <sup>f</sup>	—	—	—	—	—	—

<sup>a</sup> For designations of  $C_1$ – $C_5$  see Fig. 1. <sup>b</sup> Expectation value of the  $S^2$  operator for the wavefunction indicated in the second column (should be 0.750 for a pure doublet). <sup>c</sup> Full  $\pi$  space CAS; total atomic spin densities given (most of the spin is in  $p_\pi$ ). <sup>d</sup> Not available. <sup>e</sup> From the experimental  $a_H$  of  $C_5H_7$ <sup>29</sup> and  $C_7H_9$ ,<sup>30</sup> the values for the two terminal H atoms are averaged. <sup>f</sup> Calculation of density did not converge.

presence of higher spin states is also the reason for the underestimation of the amount of bond-length alternation in the optimized UHF geometries for polyenyl radicals.

The other methods are less plagued by spin contamination. However, on going from  $C_5H_7$  to  $C_9H_{11}$ , in the DFT calculations with the hybrid UB3LYP functional,  $\langle S^2 \rangle$  begins to deviate uncomfortably from the theoretical value of 0.75. For  $C_5H_7$  and  $C_7H_9$ , as for the ally radical, the RCCSD(T) and UCCSD(T) coupled-cluster methods predict spin distributions in the carbon  $2p_\pi$  AOs that are in closest accord with those inferred from the ratios of the observed hyperfine coupling constants. However, in all three radicals these two coupled-cluster methods both seem to underestimate slightly the relative amount of spin that appears on the terminal carbon atoms. It is not clear whether this small underestimation really does indicate a problem with these coupled-cluster methods or whether the McConnell relationship, which is used to infer the carbon  $2p_\pi$  spin distributions from the ratios of the observed hydrogen hyperfine coupling constants, is not quantitatively correct.

Because the hyperfine coupling constants have not been measured for  $C_9H_{11}$ , comparison with experiment cannot be used to judge the degree of success of the various computational methods in predicting the distribution of unpaired spin in this radical. However, since RCCSD(T) is the most successful of all the methods in predicting spin distributions in the  $C_3$ – $C_7$  radicals, it seems safe to assume that for nonatetraenyl radical RCCSD(T) provides an accurate set of  $2p_\pi$  spin densities, against which those computed by other methods can be judged. Fig. 2 compares graphically the calculated  $2p_\pi$  spin densities for  $C_9H_{11}$ ; their ratios are listed in Table 4.

Fig. 2 also shows that the CASSCF method comes closest to modelling the fall-off of the spin density towards the end of the polyenyl chain that is predicted by RCCSD(T). Both DFT methods spread the spin too evenly along the chain. This failing of the DFT methods also manifests itself in too little bond-length alternation, not only in  $C_9H_{11}$  but also in  $C_5H_7$  and in  $C_7H_9$ , as can be seen by comparing columns c and d with column h of Fig. 1 for these three radicals. UBLYP is worse than UB3LYP in predicting both the fall-off of spin density and the amount of bond-length alternation. In addition, as shown in Fig. 2 for  $C_9H_{11}$ , UBLYP gives magnitudes of positive and negative spin densities that, except at the ter-

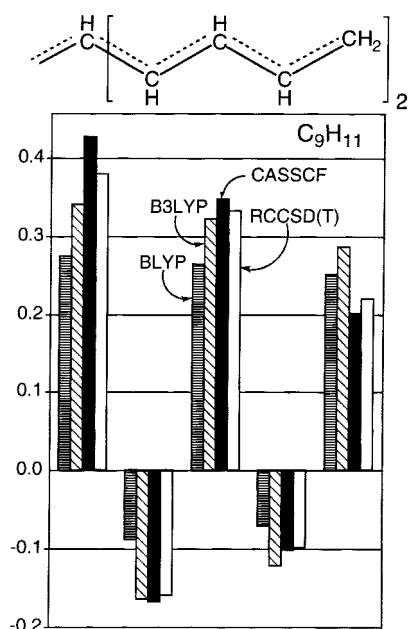


Fig. 2  $2p_\pi$  spin populations in  $C_9H_{11}$  by different methods.

minal carbon, are much smaller than those predicted by RCCSD(T).

#### 4.3. Results of calculations on $C_{11}H_{13}$ and $C_{13}H_{15}$ radicals

For radicals larger than nonatetraenyl, calculations could no longer be carried out with the apparently quite reliable coupled-cluster methods. In fact, although we were able to perform an RCCSD(T) geometry optimization for  $C_9H_{11}$ , a UCCSD(T) geometry optimization for this radical proved to be impossible to carry out with the hardware currently available to us.

Fortunately, CASSCF gives results for  $C_3$ – $C_9$  that are at least qualitatively similar to those obtained with RCCSD(T), and we found that CASSCF calculations could be carried out on somewhat larger radicals than those for which RCCSD(T) calculations were possible. We were able to perform CASSCF calculations on both  $C_{11}H_{13}$  and  $C_{13}H_{15}$ , and we used the results obtained from these calculations as benchmarks against which the DFT results on these two radicals could be compared.

We had hoped that, by excluding some  $\pi$  electrons from the active space, we might be able to perform CASSCF calculations on polyenyl radicals larger than  $C_{13}H_{15}$ . Therefore, we examined the consequences of truncating the active space for  $C_{13}H_{15}$ —the longest polyenyl radical on which we could perform CASSCF calculations with a full active space including all the spin-paired  $\pi$  electrons and a bonding and an antibonding orbital for each pair of electrons. Unfortunately, we found that the CASSCF optimized geometry changed significantly if even one pair of occupied and unoccupied MOs was deleted from the  $\pi$  active space. Consequently, the possibility of carrying out CASSCF calculations with reduced active spaces on polyenyl radicals larger than  $C_{13}H_{15}$  was not pursued further.

Fig. 3 and 4 show plots of the BLYP, B3LYP and CASSCF  $2p_\pi$  spin density distributions for  $C_{11}H_{13}$  and  $C_{13}H_{15}$ , respectively, in a format analogous to Fig. 2. The trends in Fig. 3 and 4 are similar to those in Fig. 2, with CASSCF showing the highest degree of spin localization in the central part of each of the radicals, whereas UBLYP spreads the spin almost evenly over the entire chain. The UB3LYP spin densities do attenuate from the center to the ends of the chains, but not as much as the CASSCF spin densities.

Fig. 5 shows a plot analogous to that in Fig. 1, for bond-length alternation in the  $C_{11}$  and  $C_{13}$  polyenyl radicals. Like

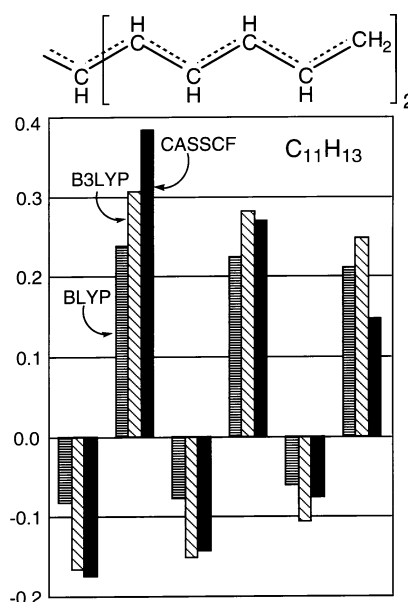


Fig. 3  $2p_\pi$  spin populations in  $C_{11}H_{13}$  by different methods.

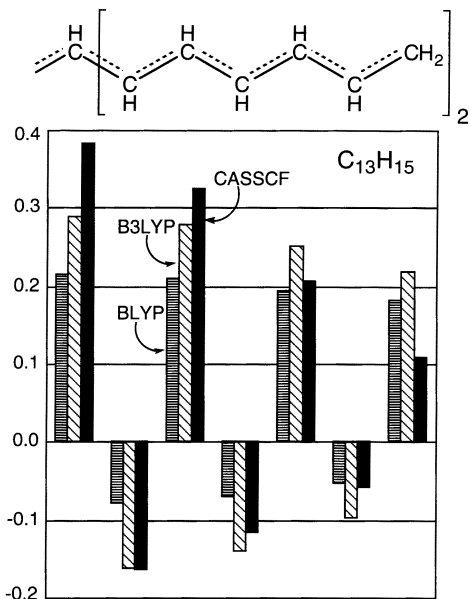


Fig. 4  $2p_x$  spin populations in  $C_{13}H_{15}$  by different methods.

Fig. 1, Fig. 5 shows that the magnitude of the difference between adjacent C–C bond lengths increases on going from the center toward the ends of the chains. This increase in the amount of bond-length alternation is largest in the CASSCF optimized geometries and least in the geometries optimized by BLYP, as expected from the observation that the CASSCF spin densities attenuate more strongly on moving from the center toward the ends of the chains than the UBLYP spin densities do.

#### 4.4. Approaching the soliton in PA—calculations on $C_{41}H_{43}$

Since the experimentally determined half-width of a neutral soliton in PA is 18 carbons,<sup>9</sup> we calculated the bond-length alternation and the spin distribution for the very long polyenyl radical,  $C_{41}H_{43}$ . Our computational results for this compound are presented diagrammatically in Fig. 6 and 7. As anticipated from the results of our calculations on smaller radicals, none of the computational methods (ROHF, UHF, UBLYP and UB3LYP) that we could apply to a polyenyl radical of this size is capable of correctly predicting the experimentally observed properties of a neutral soliton in PA. ROHF predicts the half-width of a soliton to be only about four carbon atoms (two on each side of the central carbon of the molecule); and, as shown in Fig. 6, ten carbons from the

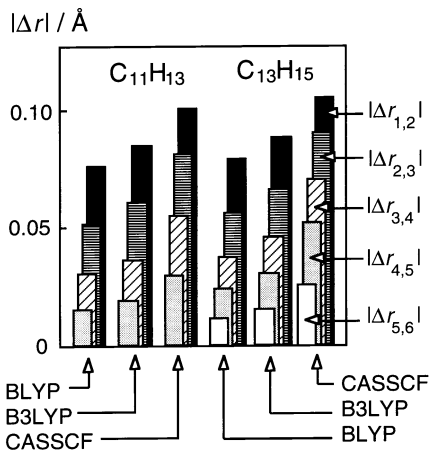


Fig. 5 Bond-length alternation in  $C_{11}H_{13}$  and  $C_{13}H_{15}$  by different methods.

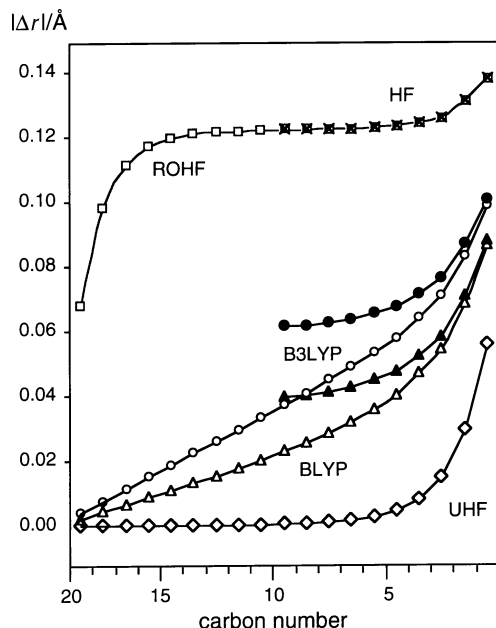


Fig. 6 Bond-length alternation pattern in  $C_{41}H_{43}$  by UHF (diamonds), ROHF (open squares), UBLYP (open triangles) and UB3LYP (open circles). The filled symbols (crosses in the case of HF) refer to the bond-length alternation pattern of the  $C_{22}H_{24}$  polyene whose origin was placed at carbon no. 10 of  $C_{41}H_{43}$ . This shows how the bond-length alternation pattern of polyenyls approaches that of polyenes towards the ends of the chain.

center the degree of bond-length alternation becomes indistinguishable from that of a polyene (crosses).

In contrast, UHF predicts that the “metallic” region, where there is no bond-length alternation, extends to within 4–5 carbons of the end of the chain, because UHF spreads the spin almost uniformly along the entire chain. As noted elsewhere,<sup>14</sup> both the ROHF and UHF methods give poor results for large radicals and, hence, are useless for performing calculations on a soliton in PA.

The two DFT-based methods do a little better, in that at least they both predict an increase in bond-length alternation and attenuation of the spin density on moving from the center

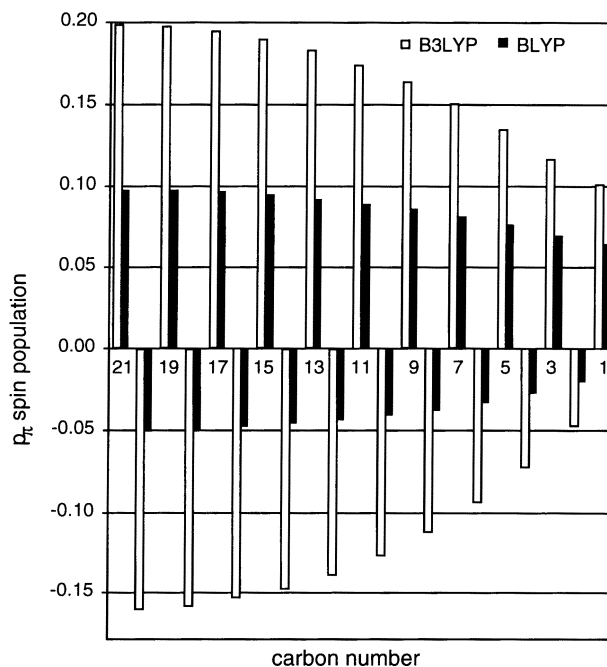


Fig. 7  $2p_x$  spin population in  $C_{41}H_{43}$  by B3LYP (open bars) and BLYP (filled bars).

toward the end of the  $C_{41}$  chain. However, this attenuation is too weak in both cases to provide an accurate model of the soliton in PA. As shown in Fig. 7, the  $2p_\pi$  spin populations are predicted by UB3LYP to fall by slightly less than 50% from the center to the end of the chain, giving a soliton width at half height of  $>40$  carbons. The fall-off from center to chain end for  $C_{41}$  is predicted to be only about 30% by UBLYP. Thus, both DFT methods predict a soliton width that is much larger than the 18 carbons found experimentally.

On the other hand, UB3LYP, with its contribution from the UHF exchange density, shows much more pronounced  $\pi$  spin polarization than UBLYP, which is a pure DFT method. In disagreement with experiment, which indicates that the ratio of the peak value of the negative to that of the positive spin density is 0.44 in all-*trans*-PA, UB3LYP predicts a value of 0.80 for this ratio; whereas UBLYP predicts a value of 0.48. Associated with the overestimation of the amount of spin polarization by UB3LYP is the fact that it predicts a value of  $\langle S^2 \rangle = 1.23$  for  $C_{41}H_{43}$ , while the BLYP value of  $\langle S^2 \rangle = 0.80$  is much closer to the correct value of  $\langle S^2 \rangle = 0.75$  for a radical.

## 5. Conclusions

In this paper we have examined various quantum chemical methods for modelling long polyenyl radicals, and, in the limit, a neutral soliton in polyacetylene (PA). We find that the coupled-cluster methods, both RCCSD(T) and UCCSD(T), do a good job of reproducing the experimental  $2p_\pi$  spin distributions in allyl, pentadienyl and heptatrienyl radicals. This judgement is based on the assumption that, as expected from the McConnell relationship, the ratios of the  $2p_\pi$  spin densities at the carbons in these radicals are the same as the ratios of the hyperfine coupling constants that have been measured for the hydrogens that are attached to the carbons.

At the RCCSD(T) and several other levels of theory, the McConnell relationship is found to hold reasonably well in the allyl radical. To within about 10%, the ratio of the calculated  $2p_\pi$  spin densities is the same as the ratio of the computed hydrogen hyperfine coupling constants ( $a_H$ ). In addition, the ratio of RCCSD(T)  $a_H$  values is very close to the ratio that has been measured by EPR experiments. However, the absolute values of the hydrogen coupling constants that are computed by RCCSD(T) and by all the other *ab initio* methods are more than 30% higher than the absolute values that have been measured.

Moreover, UCCSD(T), which gives almost exactly the same ratio of  $2p_\pi$  spin densities as RCCSD(T), gives a very different ratio of  $a_H$  values. We conclude that the *ab initio* methods that we have examined for the allyl radical do much better at computing carbon  $2p_\pi$  spin densities than at calculating absolute values of hydrogen hyperfine coupling constants and, in the case of UCCSD(T), even the ratio of  $a_H$  values.

In contrast to the wavefunction-based *ab initio* methods, the BLYP and UB3LYP versions of DFT give calculated magnitudes for the  $a_H$  values that are similar in size to the measured values; and the ratios of the calculated  $a_H$  values are nearly identical to the ratios of the  $2p_\pi$  spin densities computed at the carbons. However, the ratios of the BLYP and UB3LYP hydrogen coupling constants are farther than the RCCSD(T) ratio from the ratio of the experimental  $a_H$  values.

Comparison of the UBLYP and UB3LYP results with experiment for pentadienyl and heptatrienyl radicals, with the RCCSD(T) results for nonatrienyl, and with the CASSCF results for  $C_{11}H_{13}$  and  $C_{13}H_{15}$ , show that the falloff of spin density and increase in bond-length alternation on moving from the center toward the terminal carbons is too small. This problem is especially severe in the BLYP calculations. As a consequence of the unrealistically slow falloff of spin density in the DFT calculations, the results of the UBLYP and

UB3LYP calculations on  $C_{41}H_{43}$  show that both of these methods greatly overestimate the width of a soliton in PA.

Although our calculations on smaller polyenyl radicals indicate that *ab initio* methods such as UCCSD(T), RCCSD(T) and CASSCF are, in principle, probably capable of computing correctly at least the approximate width of a soliton in PA, in practice, UCCSD(T) could only be performed on radicals up to seven carbons in length. For RCCSD(T) the upper limit was radicals with nine carbons, and  $C_{13}H_{15}$  was the largest radical on which CASSCF calculations could be performed. Although it was possible to perform ROHF/6-31G\* and UHF/6-31G\* calculations on  $C_{41}H_{43}$ , the former *ab initio* method predicts a soliton width that is much too short and the latter a soliton width that is far too long.

Thus, we arrive at the sad conclusion that none of the above methods for performing electronic structure calculations can be successfully applied to computing properties of large polyenyl radicals, such as the width of the neutral soliton in PA. Perhaps the most promising hope for the near future is the development of functionals for DFT calculations that give correctly the falloff of spin densities in at least smaller polyenyl radicals. DFT should, in principle, be capable of computing this falloff; and DFT calculations can be performed on large polyenyl radicals which exceed the width of the neutral soliton in PA.

## Acknowledgements

This project is part of project No. 2000-053568.98 of the Swiss National Science Foundation. We thank the Swiss Center of Scientific Computing in Manno for a generous allocation of computer time on the NEC SX-4 supercomputer, without which many of the coupled cluster calculations would have been impossible to carry out. The part of this research that was performed at UW was supported by a generous grant from the U.S. National Science Foundation, which also contributed to the purchase of the cluster of IBM workstations on which some of the calculations were performed. We thank Dr. G. N. Sastry (University of Fribourg, now University of Pondicherry) for preliminary calculations on polyenyl radicals. T.B. thanks the Royal Society of Chemistry for a travel grant which allowed the pursuit of this work during a visit to Seattle.

## Supporting information

Tables containing Cartesian coordinates and total energies corresponding to the optimized geometries of all compounds discussed in this study (ASCII file) are available as ESI.†

## References

- 1 T. Ito, H. Shirakawa and S. Ikeda, *J. Polym. Sci., Polym. Chem. Ed.*, 1974, **12**, 11.
- 2 H. Shirakawa, E. J. Louis, A. G. MacDiarmid, C. K. Chiang and A. J. Heeger, *J. Chem. Soc., Chem. Commun.*, 1979, 662.
- 3 J. E. Frommer and R. E. Chance, *Encyclopedia of Polymer Science and Engineering, Second Edition*, John Wiley & Sons, New York, 1986, vol. 5, p. 462.
- 4 S. Roth and H. Bleier, *Adv. Phys.*, 1987, **36**, 285.
- 5 For the same reason, if  $C_{2v}$  symmetry is not imposed on allyl radical, at the ROHF level the unpaired electron localizes at one end of the three-carbon chain.<sup>14</sup>
- 6 D. Davidov, S. Roth, W. Neumann and H. Sixl, *Z. Phys. B*, 1983, **51**, 145.
- 7 The fact that the spins in pristine PA are associated with no charge, and the charges in lightly doped PA with no spin caused a degree of surprise and bewilderment in the solid state physics community which expressed itself in terms such as “reversed spin-charge relation” and “spinless conduction” (see e.g.: W.-P. Su, J. R. Schrieffer and A. J. Heeger, *Phys. Rev. Lett.*, 1979, **42**, 1698; W.-P. Su, J. R. Schrieffer and A. J. Heeger, *Phys. Rev. B*, 1980, **22**, 2099). To chemists, who are not used to think in terms

- of infinite systems, there is of course nothing mysterious about this
- 8 A. J. Heeger, S. Kivelson, J. R. Schrieffer and W.-P. Su, *Rev. Mod. Phys.*, 1988, **60**, 781.
  - 9 S.-I. Kuroda, *Int. J. Mod. Phys. B*, 1995, **9**, 221, and references cited therein.
  - 10 C. A. Coulson, *Proc. R. Soc. London, Ser. A*, 1938, **164**, 383.
  - 11 H. C. Longuet-Higgins and L. Salem, *Proc. R. Soc. London, Ser. A*, 1959, **251**, 172.
  - 12 J. A. Pople and S. H. Walmsley, *Mol. Phys.*, 1962, **5**, 15.
  - 13 In the SSH model,  $\beta$  is linearly dependent on the C–C bond length. The analogy between the two models is not immediately evident, because SSH chose to cast it in the algebra of second quantization.
  - 14 T. Bally and W. T. Borden, *Reviews in Computational Chemistry*, ed. K. B. Lipkowitz and D. B. Boyd, VCH-Wiley, New York, 1999, vol. 13, p. 1.
  - 15 D. Baeriswyl and K. Maki, *Phys. Rev. B*, 1985, **31**, 6633.
  - 16 D. S. Boudreaux, R. R. Chance, J. L. Brédas and R. Silbey, *Phys. Rev. B*, 1983, **28**, 6927.
  - 17 M. J. S. Dewar, J. A. Hashmall and G. G. Venier, *J. Am. Chem. Soc.*, 1968, **90**, 1953.
  - 18 L. Rodriguez-Monge and S. Larsson, *J. Chem. Phys.*, 1995, **102**, 7106.
  - 19 H. O. Villar and M. Dupuis, *Chem. Phys. Lett.*, 1987, **142**, 59.
  - 20 F. Sim, D. R. Salahub, S. Chin and M. Dupuis, *J. Chem. Phys.*, 1991, **95**, 4317.
  - 21 M. J. Frisch, G. W. Trucks, H. B. Schlegel, G. E. Scuseria, M. A. Robb, J. R. Cheeseman, V. G. Zakrzewski, J. A. Montgomery, R. E. Stratmann, J. C. Burant, S. Dapprich, J. M. Millam, A. D. Daniels, K. N. Kudin, M. C. Strain, O. Farkas, J. Tomasi, V. Barone, M. Cossi, R. Cammi, B. Menucci, C. Pomelli, C. Adamo, S. Clifford, J. Ochterski, G. A. Petersson, P. Y. Ayala, Q. Cui, L. Morokuma, D. K. Malick, A. D. Rabuck, K. Raghavachari, J. B. Foresman, J. Cioslowski, J. V. Ortiz, B. B. Stefanov, G. Liu, A. Liashenko, P. Piskorz, I. Komaromi, R. Gomperts, R. L. Martin, D. J. Fox, T. Keith, M. A. Al-Laham, C. Y. Peng, A. Nanayakkara, C. Gonzales, M. Challacombe, P. M. W. Gill, B. G. Johnson, W. Chen, M. W. Wong, J. L. Andres, M. Head-Gordon, E. S. Repogle and J. A. Pople, GAUSSIAN 98, Releases A.5 and A.7, Gaussian Inc., Pittsburgh, PA, 1998.
  - 22 K. Andersson, M. R. A. Blomberg, M. P. Fülscher, V. Kellö, R. Lindh, P.-Å. Malmqvist, J. Noga, J. Olson, B. O. Roos, A. Sadlej, P. E. M. Siegbahn, M. Urban and P.-O. Widmark, MOLCAS, 4.0, University of Lund, Sweden, 1994.
  - 23 J. F. Stanton, J. Gauss, J. D. Watts, W. J. Lauderdale and R. J. Bartlett, *Int. J. Quantum Chem.*, 1992, **26**, 879.
  - 24 M. B. Coolidge, D. A. Hrovat and W. T. Borden, *J. Am. Chem. Soc.*, 1992, **114**, 2354, and references cited therein.
  - 25 E. Hirota, C. Yamada and M. Okunishi, *J. Chem. Phys.*, 1992, **97**, 2963.
  - 26 H. M. McConnell, *J. Chem. Phys.*, 1956, **24**, 632.
  - 27 F. Gerson, *High Resolution E.S.R. Spectroscopy*, John Wiley & Sons, New York, 1978.
  - 28 A. Carrington and A. D. McLachlan, *Introduction to Magnetic Resonance*, Harper & Row, New York, 1967.
  - 29 R. Batra, B. Giese, M. Spichy, G. Gescheidt and K. N. Houk, *J. Phys. Chem.*, 1996, **100**, 18371.
  - 30 R. Sustmann and H. Schmidt, *Chem. Ber.*, 1979, **112**, 1440.
  - 31 I. G. Green and J. C. Walton, *J. Chem. Soc., Perkin Trans. 2*, 1984, 1253.